

Magnetocaloric effect in a pyrochlore antiferromagnet $\text{Gd}_2\text{Ti}_2\text{O}_7$

S. S. Sosin, L. A. Prozorova, A. I. Smirnov

P. L. Kapitza Institute for Physical Problems RAS, 119334 Moscow, Russia

A. I. Golov, I. B. Berkutov*

Department of Physics and Astronomy, University of Manchester, Manchester M13 9PL, UK

O. A. Petrenko, G. Balakrishnan

Department of Physics, University of Warwick, Coventry CV4 7AL, UK

M. E. Zhitomirsky

Commissariat à l'Énergie Atomique, DSM/DRFMC/SPSMS, 38054 Grenoble, France

(Dated: October 21, 2004)

An adiabatic demagnetization process is studied in $\text{Gd}_2\text{Ti}_2\text{O}_7$, a geometrically frustrated antiferromagnet on a pyrochlore lattice. In contrast to conventional paramagnetic salts, this compound can exhibit a temperature decrease by a factor of ten in the temperature range below the Curie-Weiss constant. The most efficient cooling is observed in the field interval between 120 and 60 kOe corresponding to a crossover between saturated and spin-liquid phases. This phenomenon indicates that a considerable part of the magnetic entropy survives in the strongly correlated state. According to the theoretical model, this entropy is associated with a macroscopic number of local modes remaining gapless till the saturation field. Monte Carlo simulations on a classical spin model demonstrate good agreement with the experiment. The cooling power of the process is experimentally estimated with a view to possible technical applications. The results for $\text{Gd}_2\text{Ti}_2\text{O}_7$ are compared to those for $\text{Gd}_3\text{Ga}_5\text{O}_{12}$, a well-known material for low temperature magnetic refrigeration.

PACS numbers: 75.30.Sg, 75.50.Ee, 75.30.Kz.

I. INTRODUCTION

The distinct feature of highly frustrated magnetic materials is a peculiar spatial arrangement of the magnetic ions. Antiferromagnets on typical geometrically frustrated structures, like, for instance, kagome, garnet, and pyrochlore lattices, have an infinite number of classical ground states. This macroscopic degeneracy precludes any type of conventional magnetic ordering. As a result, frustrated magnets remain in a disordered cooperative paramagnetic ground state at temperatures well below the paramagnetic Curie-Weiss constant θ_{CW} .^{1,2,3,4} Weak residual interactions or quantum and thermal fluctuations usually induce some kind of ordered or spin-glass state at $T^* \ll \theta_{CW}$. A number of geometrically frustrated magnets have been experimentally studied in the past decade.⁵ Magnetic pyrochlore compound $\text{Gd}_2\text{Ti}_2\text{O}_7$ is one of the prototype examples. The Gd^{3+} ions have spin $S = 7/2$ and zero orbital momentum, which yields a good realization of a nearest-neighbor Heisenberg exchange antiferromagnet on a pyrochlore lattice. Recent specific heat, susceptibility and neutron scattering measurements^{6,7,8} have shown that $\text{Gd}_2\text{Ti}_2\text{O}_7$ remains disordered over a wide temperature interval below its $\theta_{CW} \simeq 10$ K. The transition to an ordered phase is presumably driven by weak dipole-dipole interactions and occurs only at $T_{N1} \approx 1$ K.

Infinite degeneracy of the magnetic ground state of a frustrated magnet implies the presence of a macroscopic number of local zero-energy modes. Such soft modes

correspond to rotational degrees of freedom of a finite number of spins with no change in the total exchange energy. In a pyrochlore structure (a matrix of corner-sharing tetrahedra on the fcc lattice), these groups of spins are hexagons formed by the edges of neighboring tetrahedra, which lie in the kagome planes [(111) and equivalent planes] (see *e.g.* Ref. 9). In zero applied field, if the six spins are arranged antiferromagnetically around one hexagon, they effectively decouple from the other spins and can rotate by an arbitrary angle. The low-energy hexagon modes have been observed in quasielastic neutron scattering studies on spinel compound ZnCr_2O_4 , which is a spin-3/2 Heisenberg antiferromagnet on a pyrochlore lattice.⁹ The thermodynamic consequence of these local excitations is that a considerable fraction of the magnetic entropy is not frozen down to temperatures much less than θ_{CW} .

An interesting effect related to a field evolution of the zero-energy local modes is an enhanced magnetocaloric effect near the saturation field H_{sat} predicted in Ref. 10. Transformation between a nondegenerate fully polarized spin state above H_{sat} and an infinitely degenerate magnetic state below H_{sat} occurs via condensation of a macroscopic number of local modes and produces large changes of entropy in magnetic field. Quantum fluctuations do not destroy such an effect.¹¹ In particular, at $H = H_{\text{sat}}$ geometrically frustrated magnets on pyrochlore and kagome lattices have a finite macroscopic entropy, which does not depend on the value of the spin of the magnetic ions. The finite entropy of kagome an-

tiferromagnet has been calculated exactly,¹¹ whereas the corresponding quantity for a pyrochlore lattice remains unknown. Therefore, an experimental observation of the magnetocaloric effect in $\text{Gd}_2\text{Ti}_2\text{O}_7$ should be important both from a fundamental point of view, as a physical probe of the local zero-energy excitations in the frustrated ground state below H_{sat} , and because of the possible technological applications. The enhanced magnetic cooling power of gadolinium gallium garnet $\text{Gd}_3\text{Ga}_5\text{O}_{12}$ has been known for a long time,^{12,13,14} although without reference to the frustrated nature of a garnet (hyperkagome) lattice. Experiments have been also performed on other garnets.¹⁵ Thus, a comparison between the two typical frustrated magnets is important since a stronger frustration on a pyrochlore lattice produces the maximal cooling rate among all known types of geometrically frustrated magnets.¹⁰ In the present work we study experimentally and theoretically the magnetocaloric effect in $\text{Gd}_2\text{Ti}_2\text{O}_7$. Demagnetization of a $\text{Gd}_2\text{Ti}_2\text{O}_7$ sample under quasi-adiabatic conditions is performed and compared to a similar study of $\text{Gd}_3\text{Ga}_5\text{O}_{12}$. Classical Monte Carlo simulations of an ideal adiabatic demagnetization process are performed for both materials. Entropy variations and the cooling power of $\text{Gd}_2\text{Ti}_2\text{O}_7$ in an applied magnetic field are calculated from a combination of the adiabatic demagnetization results and specific heat measurements.

II. EXPERIMENT

A. Specific heat measurements

A single-crystal sample of $\text{Gd}_2\text{Ti}_2\text{O}_7$ was grown by the method described in Ref. 16 and is approximately $3.5 \times 1.5 \times 1 \text{ mm}^3$ in size (32.5 mg by mass). For preliminary estimation, we present the results of specific heat measurements of $\text{Gd}_2\text{Ti}_2\text{O}_7$ performed in a Quantum Design PPMS calorimeter at zero field and at $H = 90 \text{ kOe}$ (see Fig. 1, upper panel). The curve at $H = 0$ was taken from our previous work in Ref. 18 while the high field data were measured in the temperature range from 1.5 to 20 K. Instead of two sharp peaks on a zero field $C(T)$ dependence at $T_{N1} = 1 \text{ K}$ and $T_{N2} = 0.75 \text{ K}$ corresponding to the ordering phase transitions, the high field curve demonstrates a broad maximum around 5–6 K. The lattice contribution to the specific heat extracted by fitting the zero field data at temperatures 30–70 K in the Debye approximation is shown in the figure by a dashed line. The temperature dependence of the magnetic entropy (total entropy with the phonon part subtracted) obtained by integrating C/T curves are presented at the lower panel of Fig. 1. They give a general overview of the magnetocaloric effect in this compound. An adiabatic demagnetization of the system down to zero field starting at $H = 90 \text{ kOe}$ and $T = 10 \text{ K}$ (around θ_{CW}) results in decreasing temperature to 2 K, while the isothermal process at $T = 2 \text{ K}$ is accompanied by an entropy increase

by approximately one half of the total magnetic entropy.

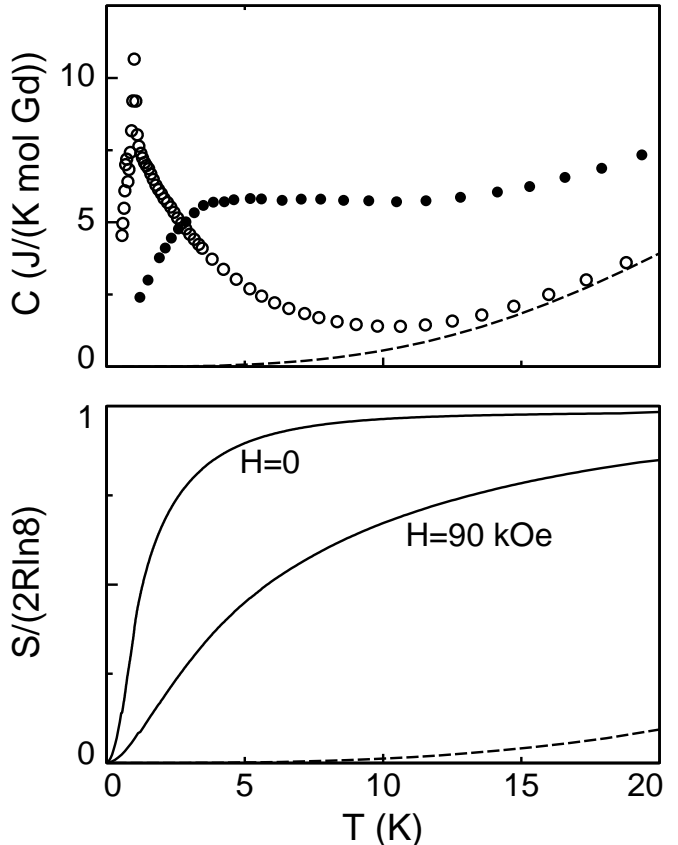


FIG. 1: Temperature dependence of the specific heat (upper panel) and the entropy (lower panel) of the $\text{Gd}_2\text{Ti}_2\text{O}_7$ single crystal sample: \circ – zero field, \bullet – $H = 90 \text{ kOe}$; solid lines are the results of C/T integration, dashed lines represent the phonon contribution.

B. Adiabatic demagnetization

In the main part of the experiment, the magnetocaloric effect in $\text{Gd}_2\text{Ti}_2\text{O}_7$ is studied in detail by measuring the temperature of the sample in a quasi-adiabatic regime as a function of time and magnetic field. For this purpose, a commercially available thin-film RuO_2 resistor with the resistance calibrated down to 100 mK in fields up to 120 kOe was glued onto the sample. It was also used as a heater to regulate the starting temperature of the experiment. The sample was suspended on four thin constantan wires ($20 \mu\text{m}$ in diameter and 5 cm in length) soldered to the thermometer to make a 4-wire resistance measurement. The experimental cell was put in a vacuum can immersed in a helium bath held at 1.8–4.2 K. The heat exchange gas inside the can was absorbed by a charcoal cryopump to a pressure of 10^{-7} torr. The cryopump was equipped with a heater to desorb some exchange gas when necessary to cool the sample during the experiment. Magnetic fields up to 120 kOe were gen-

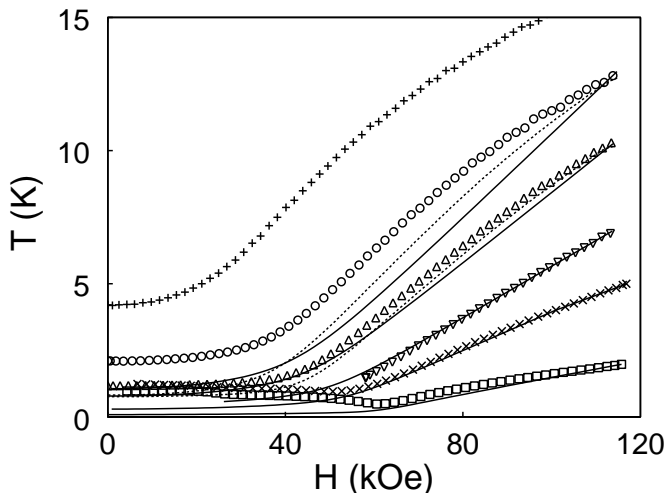


FIG. 2: Temperature variations of the adiabatic demagnetization of $\text{Gd}_2\text{Ti}_2\text{O}_7$ for various starting temperatures; dotted lines represent the corrections for the lattice heat capacity (see Discussion). Solid lines are obtained by Monte Carlo simulations with the exchange constant $J = 0.3$ K.

erated by a superconducting magnet. The field H was applied perpendicular to the (111) axis. No correction for the demagnetization factor was made. The measurements were done at a sweep rate of 10 kOe/min.

The temperature versus magnetic field curves for different starting temperatures are shown in Fig. 2. The temperature drop on demagnetization T_i/T_f depends on the starting temperature. It has a maximum around $T_i \simeq 10$ K where the temperature drops by a factor of 10. A characteristic feature for all the $T_S(H)$ curves starting below 10 K is that a great deal of cooling occurs in the field range from 120 to 60 kOe, which contrasts sharply with a continuous adiabatic cooling ($T/H = \text{const}$) of an ideal paramagnet.

Additionally, a parasitic temperature drift \dot{T}_p (due to radiation, wiring and the measuring current) was investigated at several fixed values of the field for temperatures along each curve $T_S(H)$. The values of \dot{T}_p have a smooth temperature dependence within ± 2 mK/sec changing sign at about 10 K. The experimental data were corrected at each moment of time t_0 (corresponding to each value of the magnetic field H) using a set of measured \dot{T}_p values by formula

$$T_{\text{cor}}(H, t_0) = T_{\text{exp}}(H, t_0) - \int_0^{t_0} \dot{T}_p dt, \quad (1)$$

where T_{exp} is the raw experimental value, T_{cor} is the corrected temperature. One should mention, that the above correction procedure is applicable only if the parasitic heating does not strongly affect the whole demagnetization process. In this case, after the correction is applied to the raw data, the process appeared to be fully reversible by the sweep direction, so that the curves obtained on increasing the magnetic field do not differ from

those shown in Fig. 2. A more general heat-balance equation

$$W_p dt = C dT + T (\partial S / \partial H)_T dH, \quad (2)$$

(W_p is a parasitic heat leak ($\dot{T}_p = W_p/C$), C is the specific heat at a constant field) leads to formula (1) if the function $T(\partial S / \partial H)_T / C \equiv -(\partial T / \partial H)_S$ does not change significantly between T_{exp} and T_{cor} . Such an assumption is valid for all the scans shown in Fig. 2 except the one starting at $T_i = 2$ K and the corresponding $T_S(H)$ curves are given with the appropriate subtraction. For the lowest scan, the correction appears to be of the same order of magnitude with the experimental temperature. In addition, the derivative $(\partial T / \partial H)_S$ strongly decreases in the vicinity of the ordering transition which leads to an overcorrection of the experimental data. This overcorrection is illustrated in Fig. 3 by the dashed line. Thus, an ideal adiabatic dependence $T_S(H)$ should lie between the raw experimental data and the corrected curve. The minimum temperature reached experimentally on demagnetization from $T_i = 2$ K at $H_f = 62$ kOe is $T_{\text{min}} = 0.48$ K. This cooling limit is associated with the magnetic entropy freezing at the transition into an ordered state. When the field is further decreased, a weak temperature increase is observed. Two temperature plateaus (shown by the arrows in Fig. 3) are clearly seen in this part of the curve corresponding to the phase transitions at $T_{N1} \simeq 1$ K and $T_{N2} \simeq 0.75$ K^{8,17,18}.

It is interesting to compare the above measurements to the magnetocaloric effect in another frustrated spin system $\text{Gd}_3\text{Ga}_5\text{O}_{12}$. The data on $\text{Gd}_3\text{Ga}_5\text{O}_{12}$ have been obtained on a sintered powder sample (mass 4.05 g) using an experimental technique similar to that described above. Due to the large heat capacity of the sample, no correction for parasitic heat leaks is required in this case. The measured adiabatic demagnetization curves for $\text{Gd}_3\text{Ga}_5\text{O}_{12}$ are very similar to the previously published results for oriented single crystals¹² in the temperature range of overlap. Our results are compared to $\text{Gd}_2\text{Ti}_2\text{O}_7$ data in Fig. 3 on a field scale normalized to the corresponding values of H_{sat} : 15 kOe and 70 kOe, respectively. The magnetocaloric effect in the $\text{Gd}_3\text{Ga}_5\text{O}_{12}$ sample is qualitatively similar to what is observed in $\text{Gd}_2\text{Ti}_2\text{O}_7$, but occurs in a different temperature range due to a smaller exchange constant. In a demagnetization process of $\text{Gd}_3\text{Ga}_5\text{O}_{12}$ starting from $H \simeq 2H_{\text{sat}}$ (28 kOe) at $T = 0.5$ K the temperature decreases by a factor of 5 reaching its minimum value of 0.1 K in the vicinity of the saturation field after which it remains practically constant.

III. DISCUSSION

Our experimental results demonstrate the decisive role of the frustration in producing large adiabatic temperature changes in the two materials. In typical nonfrustrated antiferromagnets, magnetocaloric ef-

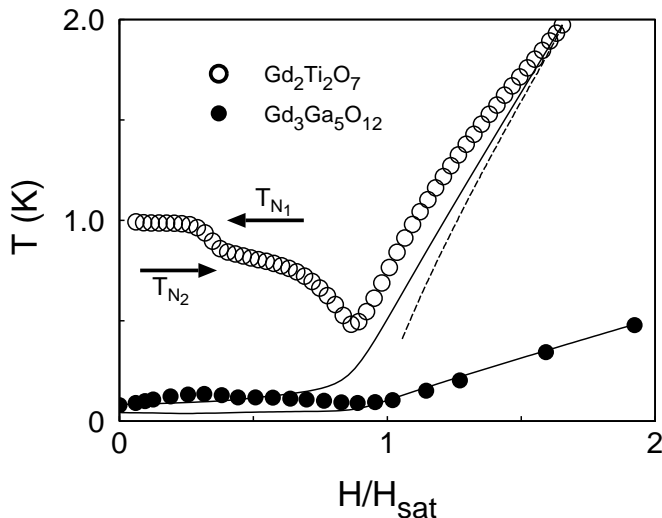


FIG. 3: Comparison of adiabatic demagnetization in $\text{Gd}_2\text{Ti}_2\text{O}_7$ (raw data) and $\text{Gd}_3\text{Ga}_5\text{O}_{12}$ on a field scale normalized to H_{sat} . Monte Carlo simulations are shown by the solid lines; the dashed line is an overcorrection to the experimental data made using formula (1).

fect in the vicinity of field induced transitions is very small. For example, adiabatic ΔT_S does not exceed 0.05 K in $\text{CsNi}_{0.9}\text{Fe}_{0.1}\text{Cl}_3$ for a similar range of fields and temperatures.¹⁹ For a quantitative description of the above data we have performed a series of Monte Carlo (MC) simulations on classical antiferromagnetic models with only nearest-neighbor exchange. A detailed account of the application of the MC technique to model adiabatic processes is given in Ref. 10. Quantum spins $S = 7/2$ are replaced by classical n -vectors ($|\mathbf{n}| = 1$), an approximation which is valid for high enough temperatures $T \gtrsim JS$. The only parameter required to compare the MC simulations to the experimental data is the exchange constant J , which is estimated from values of the saturation field or the Curie-Weiss temperature. Expressions for these quantities for nearest-neighbor antiferromagnets on pyrochlore and garnet lattices are

$$\begin{aligned} g\mu_B H_{\text{sat}} &= 8JS, & k_B \theta_{CW} &= 2JS(S+1), \\ g\mu_B H_{\text{sat}} &= 6JS, & k_B \theta_{CW} &= \frac{4}{3}JS(S+1), \end{aligned} \quad (3)$$

respectively (see, *e.g.*, Ref. 10). Corresponding values for both compounds have been taken from previous works^{6,8,17,20} and are summarized in Table I. For both materials, the exchange constants derived from H_{sat} and θ_{CW} agree to within an accuracy of $\sim 10\%$. The remaining difference may be attributed to weaker dipolar and other interactions, which are responsible for the eventual ordering in $\text{Gd}_2\text{Ti}_2\text{O}_7$ below T_{N1} and above $H = 5$ kOe in $\text{Gd}_3\text{Ga}_5\text{O}_{12}$.

The results of the MC simulations for $\text{Gd}_2\text{Ti}_2\text{O}_7$ with $J = 0.3$ K are indicated by the solid lines in Figs. 2 and 3. For the scans starting at temperatures above 10 K one can not neglect the phonon contribution to the total heat capacity of the sample. The influence of lattice

TABLE I: Experimental values H_{sat} and θ_{CW} and the estimations of the exchange constants for $\text{Gd}_2\text{Ti}_2\text{O}_7$ and $\text{Gd}_3\text{Ga}_5\text{O}_{12}$.

	H_{sat}	θ_{CW}	$J(H_{\text{sat}})$	$J(\theta_{CW})$
$\text{Gd}_2\text{Ti}_2\text{O}_7$	70 kOe	9.5 K	0.33 K	0.30 K
$\text{Gd}_3\text{Ga}_5\text{O}_{12}$	15 kOe	2.3 K	0.1 K	0.11 K

heat on the demagnetization process can be taken into account using Eq. (2), which yields the following relationship between the ideal temperature variation ΔT_S and its observed value ΔT_{real} :

$$\Delta T_S \simeq \Delta T_{\text{real}}(1 + C_{\text{ph}}/C), \quad (4)$$

where C_{ph} is the phonon part of the specific heat, C is its magnetic part. Using the results shown in Fig. 1, one can approximately correct the $T_S(H)$ curves for the temperature dependent phonon contribution (see dotted lines on Fig. 2). With this correction, the MC calculations demonstrate very good agreement with the experiment in the whole temperature range at fields above H_{sat} . Since a nearest-neighbor Heisenberg pyrochlore antiferromagnet does not order, the MC simulations cannot describe satisfactorily the observed behavior below H_{sat} at $T < 1$ K. Besides, this is also the limit of the validity of the classical approximation: $JS \simeq 1$ K. The temperature increase at $H < H_{\text{sat}}$ observed in $\text{Gd}_2\text{Ti}_2\text{O}_7$ (Fig. 3) may be attributed to the reopening of a gap in the excitation spectrum below H_{sat} caused by anisotropic interactions. The theoretical dependence obtained for $\text{Gd}_3\text{Ga}_5\text{O}_{12}$ (lower solid line in Fig. 3) with the exchange constant $J = 0.11$ K also fits the high field part of the experimental adiabatic curve very well.

Finally, we estimate the cooling power of the demagnetization process using the measured adiabatic $T_S(H)$ curves along with the specific heat data $C(T)$ obtained at high fields. The amount of heat absorbed by a magnetic material during isothermal demagnetization is related to the entropy change $\Delta Q = T\Delta S|_{H_i}^{H_f}$. Consider an adiabatic demagnetization curve, which starts at (H_i, T_i) and ends at (H_f, T_f) . The entropy along the curve $T_S(H)$ remains constant, so we can relate the entropy variations at constant temperature and in constant field:

$$\Delta S(T_f) \Big|_{H_i}^{H_f} = \Delta S(H_i) \Big|_{T_f}^{T_i} = \int_{T_f}^{T_i} C(T)/T dT. \quad (5)$$

The entropy changes ΔS of $\text{Gd}_2\text{Ti}_2\text{O}_7$ under the isothermal demagnetization at various temperatures from the initial field $H_i = 90$ kOe as a function of the final field H_f are presented by closed circles in Fig. 4. The values of ΔS are calculated from our experimental data using the above equation, while the real entropy of the system remains undefined. Two features should be underlined: (i) about one half of the total magnetic entropy

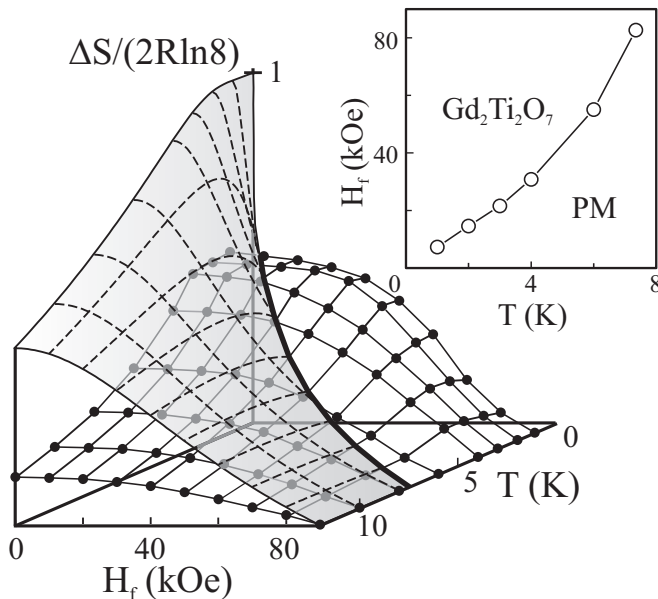


FIG. 4: The molar entropy change of $\text{Gd}_2\text{Ti}_2\text{O}_7$ under isothermal demagnetization from $H_i = 90$ kOe to H_f at different temperatures. Entropy variations of an ideal $S = 7/2$ paramagnet under the same conditions are shown by the dashed lines. The inset represents the critical intersection line of the two surfaces.

$2R \ln 8$ remains in the system even at temperatures very close to the transition into an ordered state at $T_{N1} = 1$ K; (ii) the largest entropy change ΔS and consequently, a heat absorption ΔQ occurs in a high field region above H_{sat} . This differs significantly from the behavior of an ideal paramagnet at low temperatures (shown by grey surface on Fig. 4), which releases a significant part of its entropy only if demagnetized to $H_f \ll H_i$. This figure demonstrates that $\text{Gd}_2\text{Ti}_2\text{O}_7$ has a considerable advantage below 5 K in the *high field* cooling power over conventional paramagnets. The boundary of the field-temperature area where the pyrochlore is advantageous over an ideal $S = 7/2$ paramagnet obtained as an intersection of the two sheets (the bold line) is shown in the inset to Fig. 4. For comparison, we performed similar MC simulations of a nearest-neighbor antiferromagnet (not shown in the graph). Classical models cannot give correct values for the total entropy of a quantum spin system. Nevertheless, the variation of entropy is reproduced with a remarkable accuracy. For example, the

calculated values of ΔS at $T = 4.2$ K for demagnetization from $H_i = 90$ kOe to zero field and to $H_f = 40$ kOe are 0.52 and 0.40 of the total magnetic entropy respectively. The difference from the experiment does not exceed 20%, which is due to the large $S = 7/2$ spin of the Gd^{3+} ions.

The cooling power ΔQ has a maximum around 4 K reaching 30 J/mole Gd. Such an amount of heat corresponds, for comparison, to the evaporation heat of approximately one mole of liquid ^3He at $T = 3$ K. The garnet compound $\text{Gd}_3\text{Ga}_5\text{O}_{12}$ is also advantageous as a refrigerant material over paramagnetic salts, but at lower fields and temperatures. We suggest that a combination of the two compounds might become the basis for an inexpensive two-stage adiabatic demagnetization refrigerator suitable for effective cooling from $T \sim 10$ K down to 100 mK range in a single field sweep.

IV. CONCLUSIONS

In conclusion, a large magnetocaloric effect is observed in the frustrated pyrochlore antiferromagnet $\text{Gd}_2\text{Ti}_2\text{O}_7$ in agreement with recent theoretical predictions.^{10,11} This observation points at the presence of a macroscopic number of local low-energy excitations in the vicinity of H_{sat} . Such modes can be directly probed in quasielastic neutron scattering measurements analogously to the experiment on ZnCr_2O_4 .⁹ These excitations may also be responsible for the nonfrozen spin dynamics below T_{N1} observed in $\text{Gd}_2\text{Ti}_2\text{O}_7$ by muon spin relaxation measurements.²¹ A comparison between our experimental data and classical MC simulations shows that this numerical technique can semiquantitatively predict the magnetocaloric properties of real rare-earth materials with large (semiclassical) magnetic moments, which have been described so far only in the molecular field approximation.

Acknowledgments

The authors are grateful to V. I. Marchenko and M. R. Lees for valuable discussions. This work is supported by RFBR grant 04-02-17294 and by the RF President Program. S.S.S. is also grateful to the National Science Support Foundation for the financial help.

* present address: Institute for Low Temperature Physics and Engineering, 47, Lenin av., 61103 Kharkov, Ukraine

¹ J. Villain, *Z. Phys. B* **33**, 31 (1979).

² J. T. Chalker, P. C. W. Holdsworth, E. F. Shender, *Phys. Rev. Lett.* **68**, 855 (1992).

³ R. Moessner and J. T. Chalker, *Phys. Rev. Lett.* **80**, 2929 (1998).

⁴ B. Canals and C. Lacroix, *Phys. Rev. B* **61**, 1149 (2000).

⁵ A. P. Ramirez, Geometrical Frustration, in *Handbook of Magnetic Materials* vol. 13, edited by K. H. J. Buschow (Elsevier, Amsterdam, 2001).

⁶ N. P. Raju, M. Dion, M. J. P. Gingras, T. E. Mason, and J. E. Greedan, *Phys. Rev. B* **59**, 14489 (1999).

⁷ J. D. M. Champion, A. S. Wills, T. Fennell, S. T.

- Bramwell, J. S. Gardner, and M. A. Green, Phys. Rev. B **64**, 140407(R) (2001).
- ⁸ A. P. Ramirez, B. S. Shastry, A. Hayashi, J. J. Krajewski, D. A. Huse, and R. J. Cava, Phys. Rev. Lett. **89**, 067202 (2002).
- ⁹ S.-H. Lee, C. Broholm, W. Ratcliff, G. Gasparovic, Q. Huang, T. H. Kim, and S.-W. Cheong, Nature **418**, 856 (2002).
- ¹⁰ M. E. Zhitomirsky, Phys. Rev. B **67**, 104421 (2003).
- ¹¹ M. E. Zhitomirsky and H. Tsunetsugu, Phys. Rev. B **70**, 100403(R) (2004).
- ¹² R. A. Fisher, G. E. Brodale, E. W. Hornung, and W. F. Giaque, J. Chem. Phys. **59**, 4652 (1973); E. W. Hornung, R. A. Fisher, G. E. Brodale, and W. F. Giaque, *ibid.* **61**, 282 (1974); G. E. Brodale, E. W. Hornung, R. A. Fisher, and W. F. Giaque, *ibid.* **62**, 4041 (1975).
- ¹³ J. A. Barclay and W. A. Steyert, Cryogenics **22**, 73 (1982).
- ¹⁴ B. Daudin, R. Lagnier, B. Salce, J. Magn. Mater. **27**, 315 (1982).
- ¹⁵ T. Numazava, K. Kamiya, T. Okano, and K. Matsumoto, Physica B **329-333**, 1656 (2003).
- ¹⁶ G. Balakrishnan, O. A. Petrenko, M. R. Lees, and D. McK. Paul, J. Phys. Condens. Matter **10**, L723 (1998).
- ¹⁷ P. Bonville, J. A. Hodges, M. Ocio, J. P. Sanchez, P. Vulliet, S. S. Sosin and D. Braithwaite, J. Phys.: Condens. Matter **15**, 7777 (2003).
- ¹⁸ O. A. Petrenko, M. R. Lees, G. Balakrishnan, D. McK. Paul, Phys. Rev. B **70**, 012402 (2004).
- ¹⁹ J. Wolf, K. Kiefer, M. C. Rheinstädter, K. Knorr, and M. Enderle, Eur. Phys. J. B **22**, 461 (2001).
- ²⁰ W. P. Wolf, M. Ball, M. T. Hutchings, A. F. G. Wyatt, and M. J. M. Leask, J. Phys. Soc. Jpn. Suppl. B1 **17**, 443 (1962); S. Hov, H. Bratsberg, and A. T. Skjeltorp, J. Magn. Mater. **15-18**, 455 (1980).
- ²¹ A. Yaouanc, P. Dalmas de Réotier, P. Bonville, J. A. Hodges, P. C. M. Gubbens, C. T. Kaiser and S. Sakarya Physica B **326**, 456 (2003).